New Ultraviolet Photodetector Based on Individual Nb_2O_5 Nanobelts

Xiaosheng Fang, Linfeng Hu,* Kaifu Huo,* Biao Gao, Lijuan Zhao, Meiyong Liao, Paul K. Chu, Yoshio Bando, and Dmitri Golberg*

Although human eyes are quite insensitive to ultraviolet (UV) light, most of the longer wavelength UV light (the UV-A band between 320 and 400 nm) does reach the earth surface and after prolonged exposure, the radiation can cause health concerns especially skin cancer. Therefore, it is extremely important to explore ways to effectively monitor the radiation. Herein we report for the first time a new high-performance UV photodetector made of an individual Nb_2O_5 nanobelt. Quasi-aligned Nb_2O_5 nanobelts 100–500 nm wide and 2–10 μm long were synthesized using a hydrothermal treatment of a niobium foil in a KOH solution followed by proton exchange and calcination treatment. A nanostructured photodetector was constructed from an individual Nb_2O_5 nanobelt and its optoelectronic properties were evaluated. The detector exhibited linear photocurrent characteristics, excellent light selectivity, and high external quantum-efficiency (EQE) of 6070%. Long-term stability of the photocurrent over a period of 2500 s at an applied voltage of 1.0 V was achieved. The photodetector performance was further enhanced by improving the crystallinity and eliminating the defects in the Nb_2O_5 nanobelt crystals. These excellent optoelectronic properties demonstrate that Nb_2O_5 nanobelts are suitable for visible-blind UV-light sensors and optoelectronic circuits, especially those operating in the UV-A range.

1. Introduction

Integration of functional nanodevices with low-dimensional semiconducting nanostructures is an emerging requirement and a hot nanotechnology topic.[1–3] In the past decades, extensive efforts have been made to develop various types of nanostructure-based nanodevices such as field-effect transistors (FETs),[4] photodetectors,[5] gas sensors,[6] field emitters,[7] light emission diodes (LEDs),[8] solar cells,[9] and others. In particular, as one of the most important semiconductor devices, photodetectors which convert optical signals into electrical ones have wide applications in binary switches used in imaging, light-wave communication, memory storage, and optoelectronic circuits.[10]

Compared to their bulk counterparts, one-dimensional (1D) semiconductor nanostructures generally show enhanced photosensitivity due to their high surface-to-volume ratios and reduced dimensionality.[11] The high surface-to-volume ratios can greatly increase the number of surface trapping sites, consequently prolonging the photocarrier lifetime. The reduced dimensionality can also confine the active area of the charge carriers thereby shortening the transit time.[12] Since Yang and co-workers reported an individual nanowire-based photodetector,[13] a variety of photodetectors composed of 1D semiconducting nanostructures have been fabricated and investigated.[14–20] Ultraviolet (UV) light consists of electromagnetic waves of frequencies higher than those that can be detected by the human eyes and UV radiation emitted by the sun falls in the range 200–400 nm.[21] While molecules in sunscreens and the earth's atmosphere are able to absorb most of the UV-B (290–320 nm) light and all the UV-C (200–290 nm) radiation, most of the light with the longer wavelengths, that is, the UV-A band (320–400 nm), can reach the earth's surface and prolonged exposure to UV-A may cause skin cancer. Previously reported 1D semiconductor

Prof. X. S. Fang, Dr. L. F. Hu, Dr. L. J. Zhao
Department of Materials Science
Fudan University
Shanghai 200433, P. R. China
E-mail: xshfang@fudan.edu.cn; hlf11@fudan.edu.cn
Prof. K. F. Huo, B. Gao
The Key State Laboratory Breeding Base of Refractories and Ceramics
School of Materials and Metallurgy
Wuhan University of Science and Technology
Wuhan 430081, P. R. China
E-mail: kfhuo@wust.edu.cn
Dr. M. Y. Liao
Sensor Materials Center
National Institute for Materials Science (NIMS)
Namiki 1-1, Tsukuba, Ibaraki 305-0044, Japan
Prof. P. K. Chu
Department of Physics and Materials Science
City University of Hong Kong
Tat Chee Avenue, Kowloon, Hong Kong, P. R. China
Prof. Y. Bando, Prof. D. Golberg
International Center for Materials Nanoarchitectonics (MANA)
NIMS, Namiki 1-1, Tsukuba, Ibaraki 305-0044, Japan

DOI: 10.1002/adfm.201100743

nanostructures-based UV-A photodetectors suffered from either low external quantum-efficiency (EQE) or unstable photocurrent.[22] Therefore, it is crucial to explore ways to effectively monitor UV-A radiation.

Niobium pentoxide (Nb_2O_5) which is one of the most important transition metal oxides and has promising applications in electrochemistry, catalysis, field-emission displays, and microelectronics.[23] With a bandgap of ~3.4 eV,[24] Nb_2O_5 is an ideal candidate for visible-blind UV-light sensors and optoelectronic circuits, especially those operating in the UV-A band. Moreover, it is transparent to visible light, and reliable optoelectronic performance comparable or superior to those of existing optoelectronic oxide-semiconductor-based devices can be expected from Nb_2O_5-based sensors. Nevertheless, to the best of our knowledge, there have been no studies related to the optoelectronic properties of Nb_2O_5 nanobelts. Very recently, we developed a facile topochemical process to synthesize quasi-aligned Nb_2O_5 nanobelt arrays with a controlled morphology and structure.[25] Motivated by the discovery of the unique advantages of Nb_2O_5 and our previous results,[25] we have subsequently concentrated on the optoelectronic properties of Nb_2O_5 nanobelts. A nanoscale photodetector constructed from an individual nanobelt shows high UV-A-light sensitivity, high external quantum-efficiency of 6,070%, and excellent photocurrent stability of more than 2500 s. Furthermore, superior crystallinity and optimized photodetector performance can be achieved by annealing the as-grown Nb_2O_5 nanobelts at 750 °C for 3 h under argon. These outstanding and promising optoelectronic properties demonstrate that the Nb_2O_5 nanobelts have immense potential in next-generation optoelectronic devices.

2. Results and Discussion

The X-ray diffraction (XRD) patterns of the Nb foil substrate and Nb_2O_5 nanobelt arrays grown on it are depicted in **Figure 1**a and 1b, respectively. Only two diffraction peaks at 38.5° and 55.6° are detected from the Nb foil and they correspond to the (110) and (200) reflections of Nb, respectively. These two peaks are also observed from the Nb_2O_5 nanobelt arrays (Figure 1b), albeit at a lower intensity, and all new diffraction peaks can be asigned to the monoclinic Nb_2O_5 (JCPDS No. 37-1468) with the lattice parameters of a = 20.38 Å, b = 3.824 Å, c = 19.36 Å and β = 115.69°.

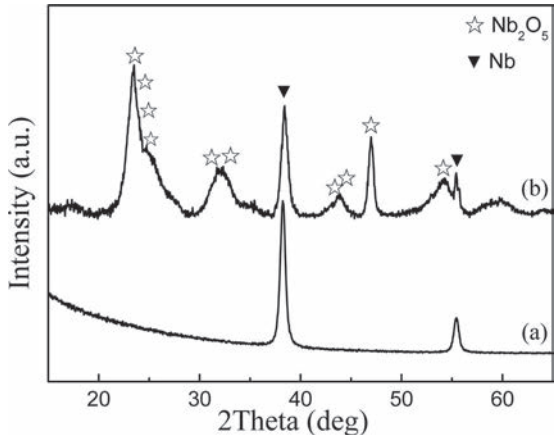

Figure 1. XRD patterns of a) Nb foil substrate and b) as grown- Nb_2O_5 nanobelt arrays on the Nb foil.

Figure 2 shows the low- and high-resolution field-emission scanning electron microscopy (SEM) images of the nanobelt sample. As shown in Figure 2a and 2b, the Nb foil is densely covered by a large number of quasi-aligned nanobelts with lengths between 2 and 10 μm and widths between 100 and 500 nm, indicating a high yield for the nanostructures. Figure 2c shows the cross-sectional SEM image of the as grown- Nb_2O_5 nanobelt arrays on the Nb foil, showing that almost all the belts are bunched together and quasi-aligned. The beltlike structure is further highlighted in Figure 2d which reveals a peculiar rectangular geometry with sharp corners and smooth surface. It is evident that the nanobelt has a uniform width along its entire length. The thickness and width of the regarded nanobelt are ~73 and ~280 nm, respectively. The energy dispersive X-ray spectrum (EDS) (Figure 2e) data acquired from an ensemble of the Nb_2O_5 nanobelt arrays confirms that the product is composed of Nb and O.

The morphology and structure of the nanobelts are further examined by transmission electron microscopy (TEM). Before conducting TEM, the nanobelts are detached from the Nb foil by sonication in ethanol and a drop of this suspension was dripped onto a C-coated copper TEM grid. The typical low-magnification TEM images in **Figure 3**a and 3b show a bundle of Nb_2O_5 nanobelts with lengths between 2 and 5 μm and within the bundlem the nanobelts are quasi-aligned. Figure 3c and 3d depict a typical TEM image of an individual belt with a uniform rectangular shape and the corresponding EDS spectrum taken from its stem, respectively. Again, only Nb and O singals are detected (Cu and C signals originating from the grid). Further investigation by X-ray photoelectron spectroscopy (XPS) reveals that the Nb_2O_5 nanobelt compositions are not stoichiometric and there are small amounts of suboxide species such as NbO_2 in the structures.[25]

The high-resolution TEM (HR-TEM) image near the edge of the nanobelt in **Figure 4**a shows clear lattice fringes perpendicular to the growth direction. The marked interplanar d spacings are ~0.34 and ~0.36 nm, corresponding to the (402) and (–405) planes of a monoclinic Nb_2O_5 crystal, respectively. A large density of stacking faults parallel to the long axis of the nanobelts is observed from the HRTEM image indicating imperfect crystallinity. Abundant stacking faults have also been observed from Nb_2O_5 nanobelts synthesized by thermal oxidation.[26] The selected-area electron diffraction (SAED) pattern taken from an individual nanobelt displays sharp diffraction spots which can be indexed to the [010] zone axis pattern (Figure 4b). During TEM observation, the nanobelts generally lay flat on the copper grid being perpendicular to the electron beam. Therefore, the observed diffraction spots of the [010] zone axis suggest that each Nb_2O_5 nanobelt is a single crystal with a (010) surface. It should be noted that the SAED pattern contains secondary spots, revealing the presence of subcrystalline domains with small-angle boundaries inside the main nanobelt crystal. Figure 4c and 4d schematically show the (402) and (–405) planes as well as atomic configuration of the belt surface. The elemental maps of an individual nanobelt are displayed in **Figure 5**. The results convey information about the

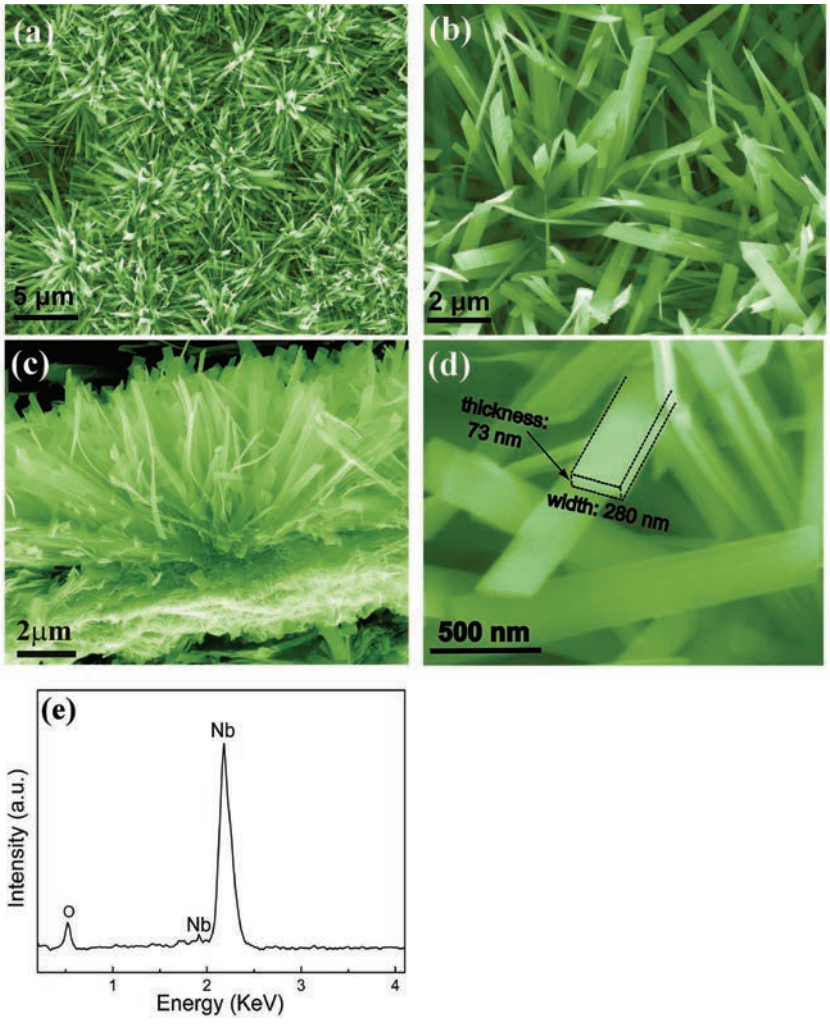

Figure 2. a) and b) Low-magnification SEM images reveal a high yield for the as-grown Nb_2O_5 nanobelt arrays. c) Cross-sectional SEM image of the as grown- Nb_2O_5 nanobelt arrays on the Nb foil, showing almost all the belts are bunched and quasi-aligned. d) Enlarged SEM images of the as-grown Nb_2O_5 nanobelt arrays. A selected nanobelt is outlined for clarity. e) The EDS spectrum taken on an ensemble of as grown- Nb_2O_5 nanobelt arrays on the Nb foil within SEM observations.

distribution of Nb and O and each element is homogeneously distributed in the structure.

To construct an individual Nb_2O_5 nanobelt-based UV photodetector, a drop containing the Nb_2O_5 nanobelts is dispersed with ethanol on a SiO_2/Si substrate. The patterned Cr (10 nm)/Au (100 nm) electrodes are deposited on the substrate which is sparsely covered by the Nb_2O_5 nanobelts using photolithography, electron-beam deposition, and the lift-off process. The schematic diagram and a typical SEM image of an individual Nb_2O_5 -nanobelt-based device configuration are exhibited in **Figure 6**a and 6b, respectively. The width of the Nb_2O_5 nanobelt and gap between the two metal electrodes are about 100 nm and 2.5 μm, respectively. Electrical characterization is performed using a two-probe method under ambient conditions and monochromatic illumination. Figure 6c presents the typical *I–V* curves obtained from the device illuminated by light of different wavelengths of 320 nm, 400 nm, 500 nm, and 600 nm as well as under dark conditions. The device shows a low dark current of 15.5 pA at an applied voltage of 1.0 V. There is no change in the photoresponsivity when the wavelengths of the light sources are 600 nm (1.68 mW/cm^2) and 500 nm (2.81 mW/cm^2) and only a small change is observed when the wavelength of the light source is changed to 400 nm (2.02 mW/cm^2). When the device is illuminated by 320 nm UV-light at 0.91 mW/cm^2, the photocurrent reaches 51.3 pA. Therefore, the present Nb_2O_5-nanobelt photodetector is much more sensitive to UV-A light than visible light, indicating a high spectral selectivity. This can be attributed to that the photogenerated carriers significantly increase the conductivity when the Nb_2O_5 nanobelt is illuminated by photons with an energy larger than its band gap (~3.4 eV, 367 nm). The approximately linear behavior of the photocurrent curve reveals the good ohmic contact between the nanobelt and electrodes. Since the surface of the nanobelts is very smooth, the clean and flat interface between the structure and electrodes ensures good electrical contact.[27] **Figure 7** displays the spectroscopic photoresponse of an individual Nb_2O_5 -nanobelt-based photodetector measured at a bias of 5 V under illumination by light of varying wavelengths from 210 nm to 600 nm. The same phenomena and mechanism described in Figure 6c is applicable to Figure 7. The significant change in the photoresponse may be due to a large density of stacking faults in the structure.

The spectra responsvity (R_λ), defined as the photocurrent generated per unit power of incident light on the effective area of a photoconductor, and the external quantum efficiency (EQE), defined as the number of electrons detected per incident photon, are two critical parameters for a photodetector. Larger values of R_λ and EQE indicate higher sensitivity and R_λ and EQE can be calculated by the following equations, respectively:[28]

$$R_\lambda = \frac{\Delta I}{PS}$$

$$EQE = \frac{hc}{e\lambda} R_\lambda$$

where ΔI is the difference between the photo-excited current and dark current, P is the light power density irradiated on the nanobelt, S is the irradiated area on an individual nanobelt, λ is the exciting wavelength, h is Planck's constant, c is the velocity of the light, and e is the electronic charge. The calculated R_λ and EQE of the present nanobelt are as high as 15.2 A/W and 6070% at an applied voltage of 1.0 V,

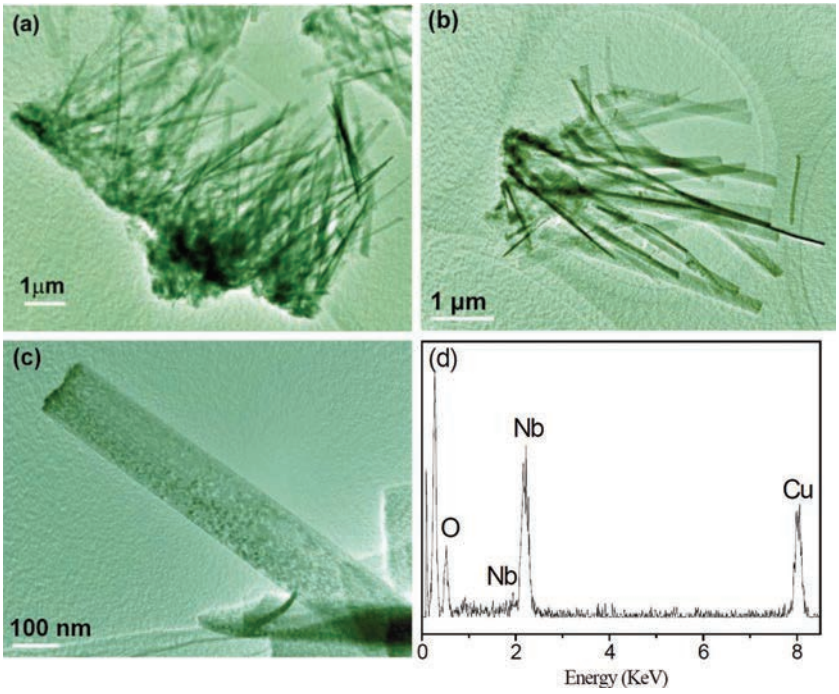

Figure 3. a, b) Two typical low-magnification TEM images of a bundle of Nb_2O_5 nanobelts showing almost all of the nanobelts are orientationally aligned. c) TEM image of a single Nb_2O_5 nanobelt and d) the corresponding EDS spectrum taken from the nanobelt stem. The Cu peak comes from the TEM grid.

respectively. The responsivity versus applied-voltage characteristic under illumination of 320 nm light is displayed in Figure 6d. For investigating the variation of the nanobelt photodetector performance (R_λ and EQE) with the nanobelt widths and illuminated areas, 10 individual Nb_2O_5 nanobelts with different widths ranging from 100 to 500 nm were constructed and measured. The observed results show that the variation in the nanobelt photodetector performance (R_λ and EQE) is small. For example, the ranges of R_λ and EQE are 14.3 to 16.6 and 5711 to 6629, respectively. The efficiency can be much higher at higher electric fields due to carrier injection. These key parameters are better or comparable to those of other existing semiconductor photodetectors as summarized in **Table 1**.[29–34]

The stability, selectivity, and sensitivity are the most important factors in sensor performance.[35] **Figure 8** depicts the variations in the photocurrent of the Nb_2O_5 nanobelt-based photodetector at 1.0 V. No obvious degradation is seen for an average photocurrent of ~52 pA over 2500 s, and the photocurrent fluctuation defined as $\Delta I/I_{average}$ is less than 5.0%, illustrating the excellent photocurrent stability. The characteristics of the present device, namely relatively high spectral selectivity, photosensitivity, and excellent photocurrent stability, etc., demonstrate that the Nb_2O_5 nanobelts are suitable for high-sensitivity UV photodetectors, especially in the UV-A band.

Considering that the Nb_2O_5 nanobelts exhibit a beltlike geometry with lengths of 2–10 μm, widths of 100–500 nm, and a thickness of several tens of nanometers thereby yielding a large surface-to-volume ratio, chemisorption on the nanobelt surface may play an important role in the photoconductive behavior. For corroboration, the response of the device under different atmospheres is investigated. As shown in **Figure 9**, the photocurrent measured at a pressure of 1 Pa is 457.7 pA, which is about 8.9 times higher than that in air (51.3 pA). The results demonstrate that the photocurrent is significantly enhanced under reduced pressure.

This result can be understood by taking into account the mechanism proposed for other *n*-type semiconducting photodetectors studied previously.[36] Oxygen molecules adsorb on the nanobelt surfaces as negatively-charged ions by capturing free electrons from the *n*-type Nb_2O_5 [O_2 (*g*) + $e^- \rightarrow O_2^-$(*ad*)] thereby creating a low-conductivity depletion region near the surface. Since the thickness of the nanobelts is rather small,

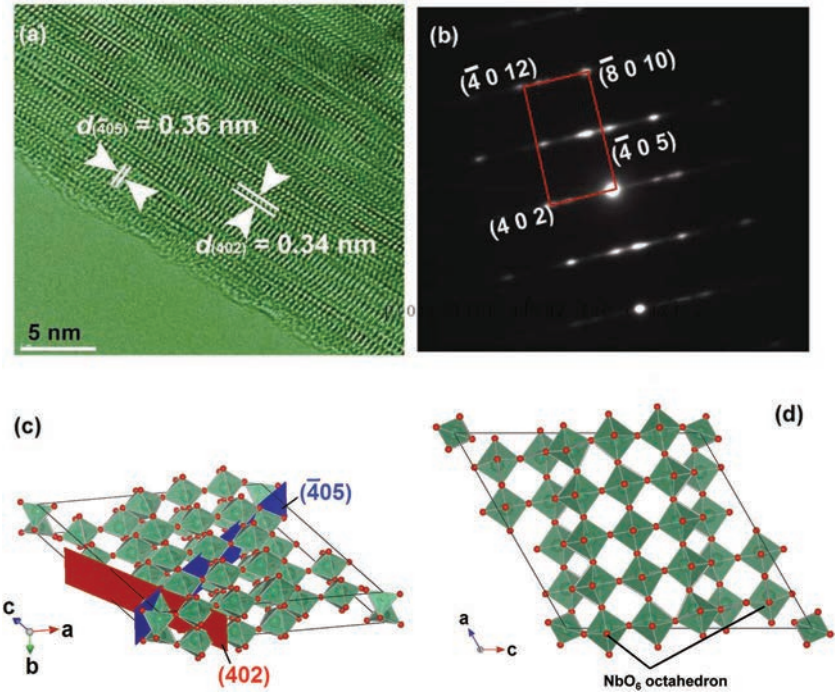

Figure 4. a, b) A lattice-resolved HRTEM image and the SAED pattern, respectively, taken from the nanobelt stem in Figure 3c. c) Side-view structure of the monoclinic Nb_2O_5 crystal to show the (402) and (–405) planes. d) Top-view structure of the monoclinic Nb_2O_5 crystal to show the atom configuration of the nanobelt surface, projection along the b axis.

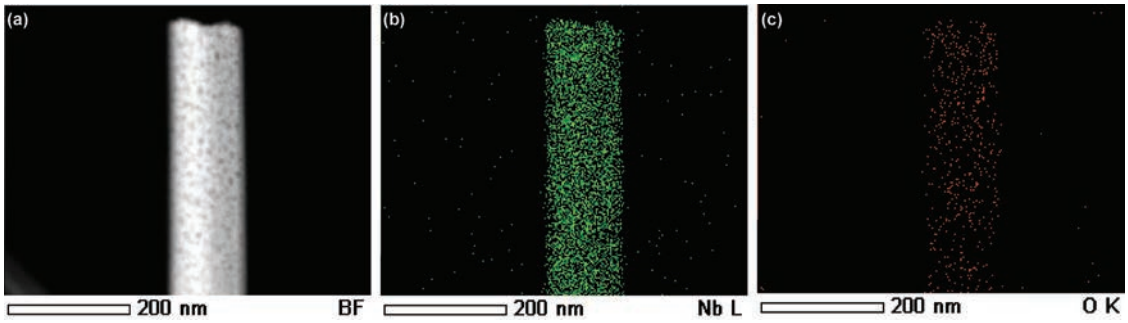

Figure 5. a) HADDF STEM image, spatially resolved EDS elemental maps depicting the distribution of the constituting elements within the nanobelt. b) Nb element, c) O element.

they are depleted with carriers and this leads to a high resistance in the dark state. Under UV illumination, the absorbed light with energy larger than the band gap will generate not only electrons in the conduction band to increase free carrier densities, but also holes with an equal density in the valence band. The holes migrate to the surface along the potential gradient and combine with oxygen to induce desorption of oxygen from the nanobelt surface [$h^+ + O_2^- (ad) \rightarrow O_2 (g)$]. This hole-trapping process increases the free carrier concentration and decreases the width of the depletion layer, leading to an apparent enhancement in the photocurrent. In vacuum, more oxygen ions can be photodesorbed from the belt surface so that the depletion region is reduced, resulting in a higher photocurrent than that in air.

It should be noted that the photocurrent under reduced pressure is 8.9 times larger than that under atmospheric pressure. This enhancement ratio is much bigger than that observed from crystalline ZrS_2 nanobelt-based or $In_2Ge_2O_7$ nanobelt-based photodetectors reported previously,[18,37] indicating that the oxygen chemisorption/desorption effect is more prominent in the present nanostructures. The enhancement ratio is reduced from 8.9 times to 5.0 times after reducing the defect density by annealing the device under argon (Ar flow rate of 80 sccm) at 750 °C for 3 h and testing in a lower pressure environment (same conditions as the original one). The results imply that this phenomenon may originate from the large density of stacking faults. Compared to the perfectly crystalline nanostructures, the large density of stacking faults in the present Nb_2O_5 nanobelt is composed of faceted areas thus providing more exposed atoms on the nanobelt surface and consequently a larger surface-to-volume ratio.

It is known that perfect crystallinity in the nanostructures usually facilitates the transport of carriers and ensures a high EQE value.[37] The morphology and microstructure shown in Figure 10a to 10c are obtained by annealing the as-grown Nb2O5 nanobelt arrays at a higher temperature of 750 °C under argon (Ar) at a flow rate of 80 standard cubic centimeter per minute (sccm). The morphology

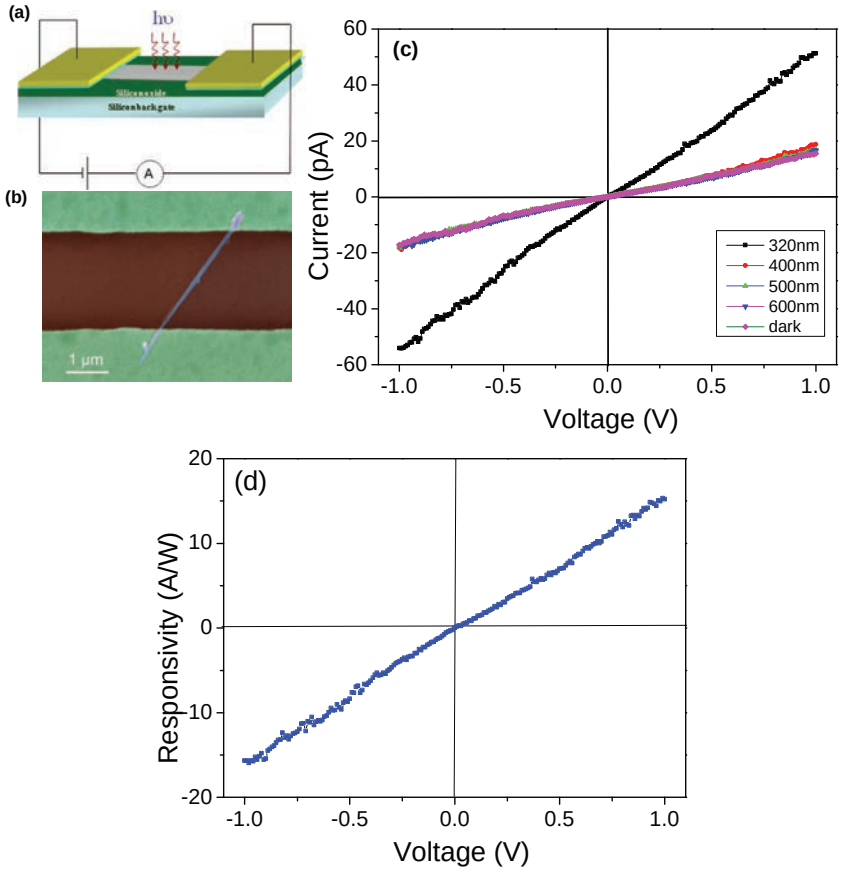

Figure 6. a, b) Schematic diagram and a SEM image of the individual Nb_2O_5-nanobelt-based device configuration, in which the Nb_2O_5 nanobelt was dispersed on a thermally oxidized Si substrate covered with a 200 nm SiO_2 layer and the Cr/Au (10 nm/100 nm) interdigitated electrodes were patterned on its top. c) The *I–V* characteristics of an individual Nb_2O_5 nanobelt photodetector illuminated with different-wavelength lights of 320 nm, 400 nm, 500 nm, and 600 nm as well as under dark conditions. d) Responsivity versus applied-voltage characteristics under illumination of 320 nm light.

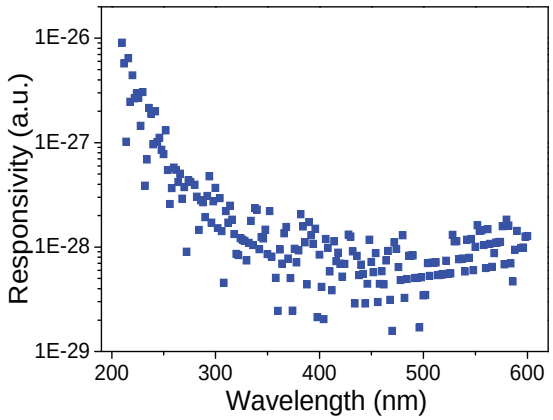

Figure 7. A spectroscopic photoresponse of an individual Nb_2O_5 nanobelt photodetector measured at a bias of 5V under the different wavelengths from 210 nm to 600 nm.

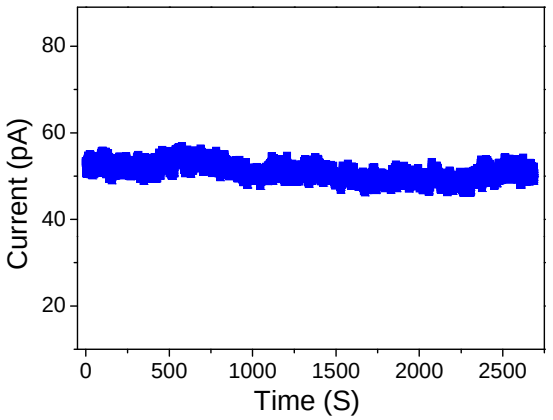

Figure 8. A photocurrent-time (I_{ph}–T) plot when an applied voltage of 1.0 V and 320 nm UV-light illumination were used.

and microstructure are not only uniform in the entire sample, but also the morphology is retained after annealing at higher temperature, as shown in Figure 10a. The lattice-resolved HR-TEM images (Figures 10b and 10c) reveal that the crystallinity of the Nb_2O_5 nanobelt is improved significantly after annealing in spite of the presence of a few defects. The photodetector performance data shown in Figures 10d and 10e are obtained by annealing the same device (shown in Figure 6b) under argon (flow rate of 80 sccm) at 750 °C for 3 h. The results demonstrat that the annealed Nb_2O_5 nanobelt photodetector with better crystallinity shows an improved photocurrent (Figure 10d) under 320 nm UV-light illumination (~100 pA at an applied voltage of 1.0 V) and a smaller dark current (~10.6 pA at an applied voltage of 1.0 V) compared to the previous one under the same measurement conditions (51.3 pA and 15.5 pA for the photocurrent and dark current, respectively). Figure 10e displays the responsivity versus applied-voltage characteristics under illumination of 320 nm light. The spectral response at 320 nm is about 37.8 A/W at a bias of 1 V, corresponding to an external quantum efficiency of 15 095%. We have very recently also produced individual nanobelt photodetectors from the annealed Nb_2O_5 nanobelts. The sensor performance is in line with our current observation by annealing the same device together with the previous one. These results demonstrate that the photodetector performance can be further optimized by improving the crystallinity and eliminating defects from the Nb_2O_5 nanobelt crystals in order to avoid the deleterious effects associated with defect and grain-boundary recombination. It further facilitates the transport of carriers in the well-defined 1D nanobelts ensuring a large active area for the charge carriers.

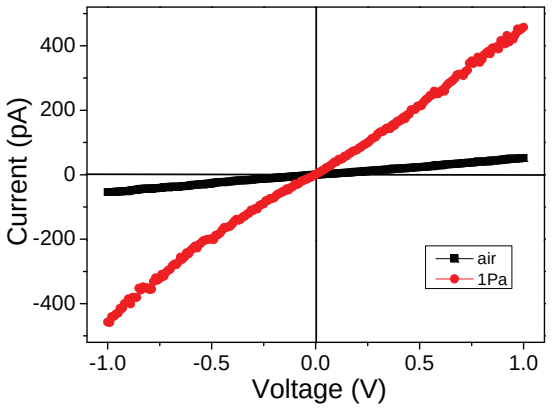

Figure 9. *I*–*V* characteristics of an individual Nb_2O_5 nanobelt photodetector illuminated with a light of 320 nm under air and vacuum conditions, respectively.

Table 1. Comparison of the critical parameters for the present Nb_2O_5 nanobelt-based and other characteristic inorganic semiconducting nanostructures-based photodetectors.

Photodetectors	R_λ	EQE	Photocurrent stability	Reference
Individual ZnS nanbelt	0.12 A/W at 5 V	50%	–	[17]
Micrometer-sacle ZnS nanobelt	–	–	1600 s	[29]
ZnSe nanobelt	0.12 A/W at 30 V	37.2%	–	[30]
Sb_2Se_3 nanowire	8.0 A/W at 5 V	1650%	–	[31]
ZnO nanowire	–	Gain ~10^8	–	[15a]
Colloidal ZnO nanoparticles	61 A/W at 120 V	–	–	[32]
TiO_2 nanocrystals and polyfluorene hybrids	6.92 mA/W at 1 V	–	–	[33]
Nanocrystalline TiO_2 thin films	199 A/W at 10 V	–	–	[34]
Nb_2O_5 nanobelt	15.2 A/W at 1 V	6070%	2500 s	Present work

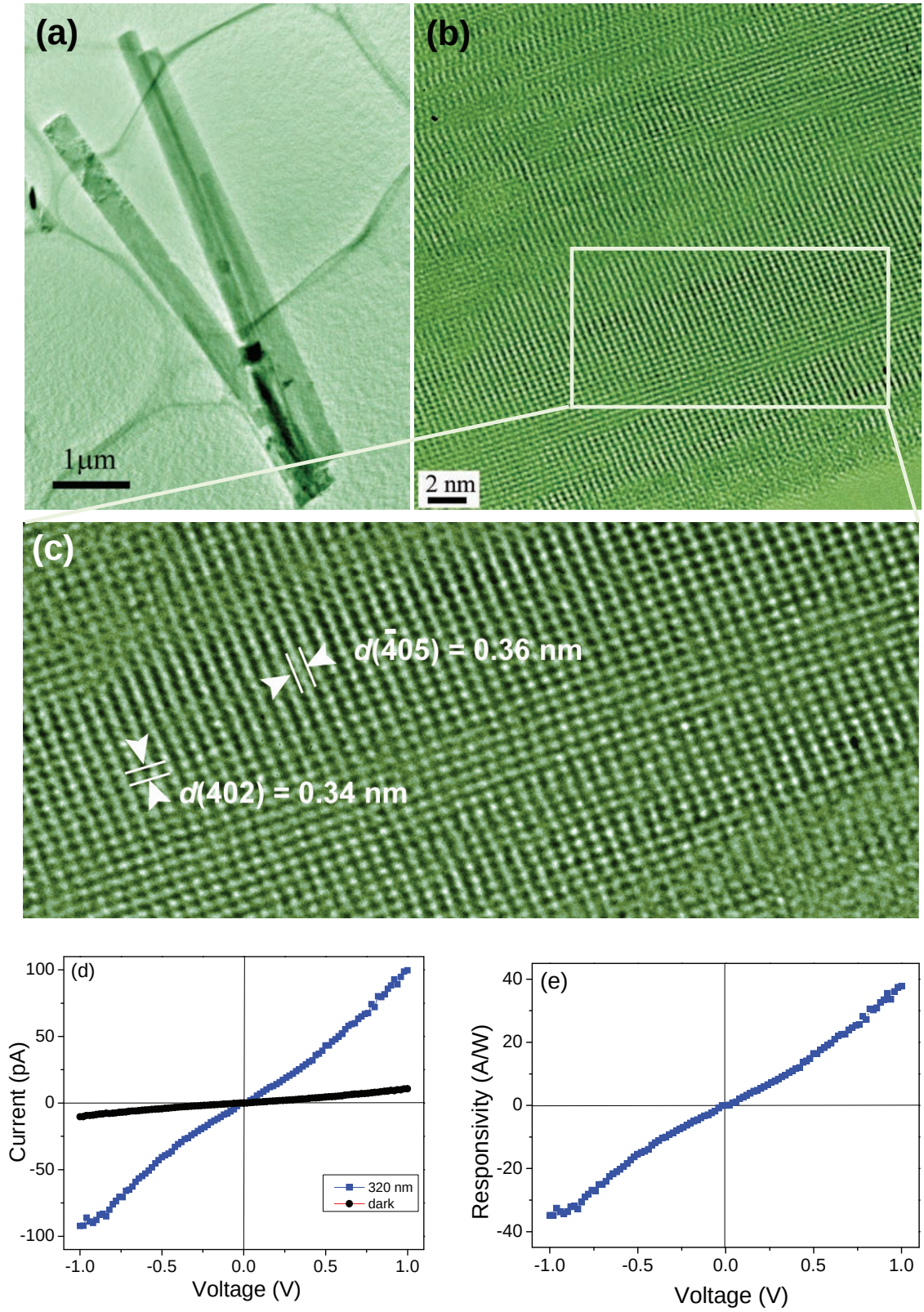

Figure 10. Morphology, microstructure and photodetector performance of the as grown- Nb_2O_5 nanobelt arrays annealed under Ar (80 sccm) at 750 °C for 3 h: a) Typical TEM image showing that the morphology does not change after annealing, b) and c) HRTEM images of a relatively large area of the nanobelt and an enlarged lattice-resolved HRTEM image taken from the marked area in (b), respectively, and d) *I–V* characteristics of an individual Nb_2O_5 nanobelt-based photodetecors illuminated by 320 nm light and under dark conditions. e) Variation of responsivity as a function of the applied voltage under illumination of 320 nm light.

3. Conclusion

The photoconductive characteristics of Nb_2O_5 nanobelts assembled into UV photodetectors are presented. The Nb_2O_5 nanobelts exhibit a high photosensitivity, light selectivity, and excellent photocurrent stability for more than 2500 s. The response and external quantum efficiency are determined to be as high as 15.2 and 6070%, respectively. The sensor performance can be further optimized by improving the crystallinity and eliminating the defects in the nanobelt crystals. The response of the device at different pressure confirms the importance of oxygen chemisorption/desorption on the surface. This novel device composed of Nb_2O_5 nanobelts has potential in next-generation photosensors and photodetectors.

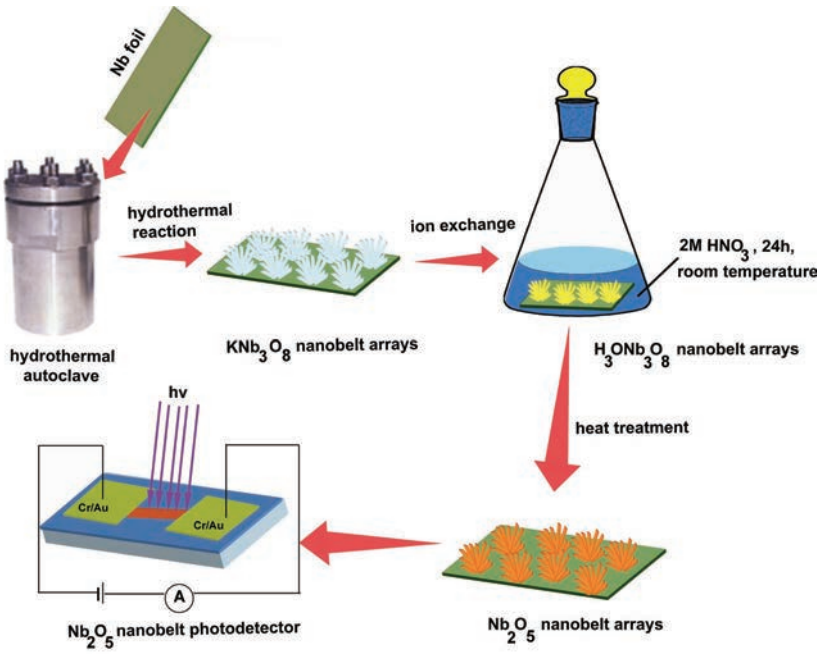

Scheme 1. Schematic illustration of the fabrication procedure of Nb_2O_5 nanobelt photodetector.

4. Experimental Section

Typically, a commercial niobium foil (Nb, 99.99%, Baoji Refractory Metal Company, Baoji, China) 1 cm × 1 cm in size was polished with SiC sandpaper, ultrasonically cleaned with acetone, ethanol, and deionized water for 5 min sequentially, and dried under flowing N_2. The Nb foil was immersed in 40 mL of 0.02 mol/L KOH solution in a 60 mL Teflon-lined stainless steel autoclave. The autoclave was sealed and heated to 170 °C for 16 h and cooled naturally to room temperature after the reaction. The processed Nb foil covered by a white product was taken out and further immersed in a 2 mol/L HNO_3 solution for 24 h at room temperature. The protonated products underwent ion exchange, was rinsed to a neutral pH with deionized water, dried at room temperature, and calcined for 3 h at 650 °C under Ar flow to obtain a white product consisting of Nb_2O_5 nanobelts.[25]

An individual Nb_2O_5 nanobelt-based UV photodetector was constructed from an individual nanobelt using the following procedure. Firstly, the as-grown Nb_2O_5 nanobelts were detached from the Nb foil ultrasonically in ethanol over 5 min and a drop of this dispersion was dried on a Si substrate with a 200-nm SiO_2 top layer. The Cr/Au (10 nm/100 nm) electrodes were patterned on the top of the nanobelts using photolithography, electron-beam deposition, and the lift-off process.[22a] The procedures are schematically illustrated in **Scheme 1**.

The morphology, structure, and composition of the samples were determined by X-ray diffraction using Cu K_α radiation (λ = 1.5418 Å) (XRD, Philips X' Pert Pro), field-emission scanning electron microscopy (SEM, FEI Nova 400 Nano), and transmission electron microscopy (TEM, JEOL 2010 equipped with X-ray energy dispersive spectrometry (EDS). The current-voltage (*I*–*V*) characteristics of the photodetectors were measured using an Advantest Picoammeter R8340A and a DC voltage source R6144.

Acknowledgements

This work was supported by the National Natural Science Foundation of China (Grant Nos. 51002032, 21001028 and 50902104), Shanghai Pujiang Program, Shanghai Chenguang Foundation (11CG06), the Ministry of Science and Technology of China, the innovative team of Ministry of Education of China (IRT0911), Grants-in-Aid for Scientific Research (B), Japan Society for the Promotion of Science (JSPS) (No. 22760517), the World Premier International Research Center (WPI) Initiative on Materials Nanoarchitectonics (MANA), MEXT, Japan, City University of Hong Kong Research Grant No. 9360110, and City University of Hong Kong Strategic Research Grant (SRG) No. 7008009.

Received: April 3, 2011
Revised: May 19, 2011
Published online: September 8, 2011

[1] a) C. M. Lieber, Z. L. Wang, *MRS Bull.* **2007**, *32*, 99; b) L. Li, P. Wu, X. S. Fang, T. Y. Zhai, L. Dai, M. Y. Liao, Y. Koide, H. Q. Wang, Y. Bando, D. Golberg, *Adv. Mater.* **2010**, *22*, 3161; c) X. S. Fang, T. Y. Zhai, U. K. Gautam, L. Li, L. M. Wu, Y. Bando, D. Golberg, *Prog. Mater. Sci.* **2011**, *56*, 175.
[2] a) Z. L. Wang, J. H. Song, *Science* **2006**, **14**, 242; b) U. K. Gautam, L. S. Panchakarla, B. Dierre, X. S. Fang, Y. Bando, T. Sekiguchi, A. Govindaraj, D. Golberg, C. N. R. Rao, *Adv. Funct. Mater.* **2009**, *19*, 131.
[3] a) Q. F. Zhang, C. S. Dandeneau, X. Y. Zhou, G. Z. Cao, *Adv. Mater.* **2009**, *21*, 4087; b) U. K. Gautam, M. Imura, C. S. Rout, Y. Bando, X. S. Fang, B. Dierre, L. Sakharov, A. Govindaraj, T. Sekiguchi, D. Golberg, C. N. R. Rao, *Proc. Natl. Acad. Sci. USA* **2010**, *107*, 13588.
[4] Y. Ahn, J. Dunning, J. Park, *Nano Lett.* **2005**, *5*, 1367.
[5] a) J. J. Wang, Y. Q. Wang, F. F. Cao, Y. G. Guo, L. J. Wan, *J. Am. Chem. Soc.* **2010**, *132*, 12218; b) Y. B. Li, T. Tokizono, M. Y. Liao, M. A. Zhong, Y. Koide, I. Yamada, J. J. Delaunay, *Adv. Funct. Mater.* **2010**, *20*, 3972; c) Y. G. Han, G. Wu, H. G. Li, M. Wang, H. Z. Chen, *Nanotechnology* **2010**, *21*, 185708; d) C. Soci, A. Zhang, X. Y. Bao, H. Kim, Y. Lo, D. L. Wang, *J. Nanosci. Nanotechnol.* **2010**, *10*, 1430.
[6] a) M. Law, H. Kind, F. Kim, B. Messer, P. D. Yang, *Angew. Chem. Int. Ed.* **2002**, *41*, 2405; b) S. J. Pearton, F. Ren, Y. L. Wang, B. H. Chu, K. H. Chen, C. Y. Chang, W. Lim, J. S. Lin, D. P. Norton, *Prog. Mater. Sci.* **2010**, *55*, 1.
[7] a) X. S. Fang, Y. Bando, U. K. Gautam, C. H. Ye, D. Golberg, *J. Mater. Chem.* **2008**, *18*, 509; b) Z. G. Chen, J. Zou, D. W. Wang, L. C. Yin,

G. Liu, Q. F. Liu, C. H. Sun, X. D. Yao, F. Li, X. L. Yuan, T. Sekiguchi, G. Q. Lu, H. M. Cheng, *Adv. Funct. Mater.* **2009**, *19*, 484.
[8] Y. Huang, X. F. Duan, C. M. Lieber, *Small* **2005**, *1*, 142.
[9] a) Y. H. Yu, P. V. Kamat, M. Masuru, *Adv. Funct. Mater.* **2010**, *20*, 1464; b) B. D. Weil, S. T. Connor, Y. Cui, *J. Am. Chem. Soc.* **2010**, *132*, 6642; c) C. Tao, S. P. Ruan, G. H. Xie, X. Z. Kong, L. Shen, F. X. Meng, C. X. Liu, X. D. Zhang, W. Dong, W. Y. Chen, *Appl. Phys. Lett.* **2009**, *94*, 043311; d) K. Sun, Y. Jing, N. Park, C. Li, Y. Bando, D. L. Wang, *J. Am. Chem. Soc.* **2010**, *132*, 15465.
[10] a) F. Xia, T. Mueller, Y. Lin, A.V. Garcia, P. Avouris, *Nat. Nanotech.* **2009**, *4*, 839; b) G. Konstantatos, E. H. Sargent, *Nat. Nanotech.* **2010**, *5*, 391.
[11] a) Y. N. Xia, P. D. Yang, Y. G. Sun, Y. Y. Wu, B. Mayers, B. Gates, Y. Yin, F. Kim, H. Yan, *Adv. Mater.* **2003**, *15*, 353; b) L. D. Zhang, M. Fang, *Nano Today* **2010**, *5*, 128; c) Y. Z. Jin, R. J. Curry, J. Sloan, R. A. Hatton, L. C. Chong, N. Blanchard, V. Stolojan, H. W. Kroto, S. R. P. Silva, *J. Mater. Chem.* **2006**, *16*, 3715.
[12] S. Liu, J. F. Ye, Y. Cao, Q. Shen, Z. F. Liu, L. M. Qi, X. F. Guo, *Small* **2009**, *4*, 2371.
[13] H. Kind, H. Yan, B. Messer, M. Law, P. D. Yang, *Adv. Mater.* **2002**, *14*, 158.
[14] R. Yang, Y. L. Chueh, J. R. Morber, R. Snyder, L. J. Chou, Z. L. Wang, *Nano Lett.* **2007**, *7*, 269.
[15] a) C. Soci, A. Zhang, B. Xiang, S. A. Dayeh, D. P. R. Aplin, J. Park, X. Y. Bao, Y. H. Lo, D. Wang, *Nano Lett.* **2007**, *7*, 1003; b) Y. Jiang, W. J. Zhang, J. S. jie, X. M. Meng, X. Fan, S. T. Lee, *Adv. Funct. Mater.* **2007**, *17*, 1795.
[16] Q. Wan, E. Darroli, W. Lu, *Small* **2008**, *4*, 451.
[17] J. J. Wang, F. F. Cao, L. Jiang, Y. G. Guo, W. P. Hu, L. J. Wan, *J. Am. Chem. Soc.* **2009**, *131*, 15602.
[18] L. Li, X. S. Fang, T.Y. Zhai, M. Y. Liao, U. K. Guatam, X. C. Wu, Y. Koide, Y. Bando, D. Golberg, *Adv. Mater.* **2010**, *22*, 4151.
[19] a) D. Wei, Y. Liu, L. Cao, H. Zhang, L. Huang, G. Yu, *Chem. Mater.* **2010**, *22*, 288; b) Y. J. Zhang, J. J. Wang, H. F. Zhu, H. Li, L. Jiang, C. Y. Shu, W. P. Hu, C. R. Wang, *J. Mater. Chem.* **2010**, *20*, 9858.
[20] a) Y. J. Yoon, K. S. Park, J. H. Heo, J. G. Park, S. Nahm, K. J. Choi, *J. Mater. Chem.* **2010**, *20*, 2386; b) L. F. Hu, J. Yan, M. Y. Liao, L. M. Wu, X. S. Fang, *Small* **2011**, *7*, 1012.
[21] X. S. Fang, Y. Bando, U. K. Gautam, T. Y. Zhai, H. B. Zeng, X. J. Xu, M. Y. Liao, D. Golberg, *Crit. Rev. Solid State Mater. Sci.* **2009**, *34*, 190.
[22] a) X. S. Fang, Y. Bando, M. Y. Liao, U. K. Gautam, C. Y Zhi, B. Dierre, B. D. Liu, T. Y. Zhai, T. Sekiguchi, Y. Koide, D. Golberg, *Adv. Mater.* **2009**, *21*, 2034; b) W. S. Wang, T. T. Wu, T. H. Chou, Y. Y. Chen, *Nanotechnology* **2009**, *19*, 135503.
[23] a) N. Ozer, D. G. Chen, C. M. Lampert, *Thin Soild Films* **1996**, *277*, 162; b) M. Zumer, V. Nemanic, B. Zajec, M. Remskar, A. Mrzel, D. Milhailovic, *Appl. Phys. Lett.* **2004**, *84*, 3615; c) M. Mozetic, U. Cvelbar, M. K. Sunkara, S. Vaddiraju, *Adv. Mater.* **2005**, *17*, 2138; d) M. C. Orilall, N. M. Abrams, J. Lee, F. J. Disalvo, U. Wiesner, *J. Am. Chem. Soc.* **2008**, *130*, 8882.
[24] K. Yoshimura, T. Miki, S. Iwama, S. Tanemura, *Thin Solid Films* **1996**, *282*, 235.
[25] B. Gao, J. Fu, K. Huo, W. Zhang, Y. Xie, P. K. Chu, *J. Am. Ceram. Soc.* DOI: 10.1111/j.1551-2916.2010.04370.x.
[26] B. Varghese, S. C. Haur, C. T. Lim, *J. Phys. Chem. C* **2008**, *112*, 10008.
[27] X. Zhang, J. Jie, W. Zhang, C. Zhang, L. Luo, Z. He, X. Zhang, W. Zhang, C. Lee, S. T. Lee, *Adv. Mater.* **2008**, *20*, 2427.
[28] a) J. P. Chen, Y. J. Zhang, R. Y. Guo, *J. Cryst. Growth* **2008**, *310*, 57; b) X. P. Chen, H. L. Zhu, J. F. Cai, Z. Y. Wu, *J. Appl. Phys.* **2007**, *102*, 024505; c) T. Y. Zhai, H. M. Liu, H. Q. Li, X. S. Fang, M. Y. Liao, L. Li, H. S. Zhou, Y. Koide, Y. Bando, D. Golberg, *Adv. Mater.* **2010**, *22*, 2547.
[29] X. S. Fang, Y. Bando, M. Y. Liao, T. Y. Zhai, U. K. Gautam, L. Li, Y. Koide, D. Golberg, *Adv. Funct. Mater.* **2010**, *20*, 500.
[30] X. S. Fang, S. L. Xiong, T. Y. Zhai, Y. Bando, M. Y. Liao, U. K. Gautam, Y. Koide, X. G. Zhang, Y. T. Qian, D. Golberg, *Adv. Mater.* **2009**, *21*, 5016.
[31] T. Y. Zhai, M. F. Ye, L. Li, X. S. Fang, M. Y. Liao, Y. F. Li, Y. Koide, Y. Bando, D. Golberg, *Adv. Mater.* **2010**, *22*, 4530.
[32] H. L. Xue, X. Z. Kong, Z. R. Liu, C. X. Liu, J. R. Zhou, W. Y. Chen, S. P. Ruan, Q. Xu, *Appl. Phys. Lett.* **2007**, *90*, 201118.
[33] Y. Z. Jin, J. P. Wang, B. Q. Sun, J. C. Blakesley, N. C. Greenham, *Nano Lett.* **2008**, *8*, 1649.
[34] Y. G. Han, G. Wu, M. Wang, H. Z. Chen, *Polymer* **2010**, *51*, 3736.
[35] a) X. J. Huang, Y. K. Choi, *Sens. Actuators, B* **2007**, *122*, 659; b) X. S. Fang, L. F. Hu, C. H. Ye, L. D. Zhang, *Pure Appl. Chem.* **2010**, *82*, 2185.
[36] a) T. Gao, Q. H. Li, T. H. Wang, *Appl. Phys. Lett.* **2005**, *86*, 173105; b) J. Zou, Q. Zhang, K. Huang, N. Marzari, *J. Phys. Chem. C* **2010**, *114*, 10725.
[37] L. Li, P. S. Lee, C. Y. Yan, T. Y. Zhai, X. S. Fang, M. Y. Liao, Y. Koide, Y. Bando, D. Golberg, *Adv. Mater.* **2010**, *22*, 5145.